Integration of Arbitrary Lumped Multiport Circuit Networks Into the Discontinuous Galerkin Time-Domain Analysis

Ping Li, *Student Member, IEEE*, and Li Jun Jiang, *Senior Member, IEEE*

***Abstract*—A hybrid electromagnetic (EM) circuit simulator is proposed for incorporating multiport lumped circuit networks through their admittance matrices into the discontinuous Galerkin time-domain (DGTD) method. The admittance matrix in the Laplace domain can be derived analytically or obtained from network parameters such as S-parameters in the frequency domain. To convert frequency-dependent S-parameters into the admittance matrix in the Laplace domain, the vector-fitting technique is employed to facilitate the mapping process. The computational domain of interest is split into two subdomains. One is the EM part solved by the DGTD, and another is the circuit part modeled by the basic *I–V* relationships in the time domain. The couplings between the EM and circuit parts happen at lumped ports where the port voltages and currents are solved via these coupled systems. Due to the local properties of DGTD operations, only small coupling matrix equation systems are involved. To further improve the efficiency, local time-stepping strategy is included. To show the validity of the proposed simulator, several numerical examples are presented and compared with results from other references.**

***Index Terms*—Circuit network parameters, discontinuous Galerkin time-domain (DGTD) method, fast-relaxation vector-fitting (FRVF) method, local time-stepping (LTS) method, multiport lumped-circuit networks, transient analysis.**

I. Introduction

THE ever-increasing operating frequencies of electronic circuits and the continuous minimization of the packaging size require the considerations of unintentional electromagnetic (EM) emissions to ensure a successful system design. Pure circuit simulations [1] based on circuit theory lacks the ability to combine the radiation effect into the simulation process. On the other hand, a full-wave simulator is able to take into account the EM radiation effect by solving Maxwell's and circuit equations simultaneously. Generally, there are two major methods to incorporate the lumped networks. One is using network parameters such as circuit scattering or admittance matrices [2]–[4], [13] to represent the complex circuit networks. Another one is using SPICE-like models [12], [14], [19] to replace the networks. Compared with SPICE-like models, network-parameter-based methods have genuine advantages since lumped circuit systems could have been pre-designed and characterized in terms of the measured or simulated S-parameters. In this case, lumped circuit networks are regarded as black boxes. This is ideal for confidential purposes to avoid disclosing Internet protocol (IP) details.

Compared with frequency-domain methods, time-domain methods have inherent merits since they can characterize the broadband properties through a single simulation. Among various available time-domain full-wave methods, the finite-difference time-domain (FDTD) is popular for its direct solution of Maxwell's equations in the time domain [10]. Recently, FDTD has been applied to model lumped circuit networks [2]–[9]. The lumped elements in the circuit network are treated through a direct stamping approach [5], [6] by assigning each element into an edge of the FDTD grid, or using equivalent voltage/current source concepts [7]–[9] to represent the entire network. Another approach is by transforming the admittance matrix in the Laplace domain to the time domain using the fact that the division of the current or voltage by the state variable s ($s = j\omega$) in the s-domain is an integral operation in the time domain [3], [4].

To model complex geometries with higher order accuracy, the time-domain finite-element method (TDFEM) [11] is another good candidate. Similar to the FDTD, the TDFEM has also been extended to solve antenna, electrical packaging, and circuit problems [12]–[14]. The TDFEM combined with a SPICE-like transient solver modified nodal analysis (MNA) [33] is developed [12], [14]. In [13], the TDFEM is coupled with lumped circuit networks represented by admittance matrix in the Laplace domain. In these references, the entire computational domain is split into two parts. One is the EM part and another is the circuit domain. The EM part is solved by the TDFEM, while the circuit subsystem is analyzed by circuit solvers. The interaction between the EM and circuit subsystems happens at the lumped port residing over the finite-element method (FEM)-based mesh edges. When only measured networks parameters are known, vector fitting is employed to approximate the admittance element by rational functions [13]. To further improve the effi-

Manuscript received January 10, 2013; revised April 23, 2013; accepted April 25, 2013. Date of publication May 16, 2013; date of current version June 28, 2013. This work was supported by the Research Grants Council of Hong Kong under Grant GRF 713011 and Grant GRF 712612 and by the National Science Foundation of China under Grant NSFC 61271158. This work was supported in part by the University Grants Council of Hong Kong under Contract AoE/P-04/08.

The authors are with the Department of Electrical and Electronic Engineering, University of Hong Kong, Hong Kong (e-mail: liping@eee.hku.hk; jianglj@hku.hk).

Color versions of one or more of the figures in this paper are available online at http://ieeexplore.ieee.org.

Digital Object Identifier 10.1109/TMTT.2013.2261085

ciency of the hybrid solver, a flexible time-marching scheme deploying different time-step size for the circuit and field subsystems is adopted in [26].

The discontinuous Galerkin time-domain (DGTD) method [15]–[22] is a promising approach, which is the combination of the finite-volume method [23] and FEM [11]. It supports various types and shapes of elements and unstructured meshes. It can easily achieve $h-p$ refinement. Due to the local property of the DGTD, the solution is allowed to be discontinuous across boundary faces between neighboring elements. The communication between adjacent elements is achieved via the numerical flux. In this way, the resultant mass matrix is locally coupled with the dimension equal to the number of degrees of freedom in that element. It can be regarded as an element-level domain-decomposition method and solved element by element with a fully explicit time-marching scheme. In [16] and [17], the DGTD is applied to study the transient behavior of interconnect structures with simple linear R, L, and C lumped elements. Each lumped element is treated through a FDTD-like direct stamping approach by assigning each of them to a rectangular impedance surface. For this kind of direct stamping method, it lacks the flexibility to tackle complex circuit networks. In [18], the lumped network is solved by a direct call of the external commercial circuit simulator SPICE, while [19] developed a hybrid field-circuit by exploiting the DGTD and MNA to handle single lumped port circuits.

For approaches in [17]–[19], details of circuit networks must be known in advance. However, there are many situations where only network parameters like S- or Y-parameters are provided. In this paper, an algorithm for incorporating circuit networks based on the admittance matrix in the Laplace domain into the DGTD is proposed [4], [13]. To the authors' knowledge, such an algorithm has never been reported in the DGTD literature. To solve the hybrid distributive and lumped system, the whole computational system is divided into two subsystems: one is the EM subsystem, and another is the circuit subsystem. The EM subsystem is analyzed by solving two first-order Maxwell's equations with the DGTD, and the circuit subsystem is modeled by the IV relationship based on the time-domain admittance matrix. The lumped port residing over an impedance surface is defined at the interface between the EM and circuits subsystems. The EM-to-circuit coupling is facilitated by introducing an external port voltage source computed by the EM solver, while the circuit-to-EM coupling is realized by introducing a port current source calculated through the circuit solver. This coupled EM-circuit system matrix is local with the dimension equal to the number of degrees of freedom for the $\mathbf{E}$-field in the mesh cell plus the number of port voltage and current. When multiscale meshes are involved, in our approach, the local time-stepping (LTS) [25] strategy is applied to the proposed algorithm.

The organization of this paper is as follows. The theory and formulation of the proposed algorithm is described in Section II. It includes the formulation of the DGTD, the circuit system equations, and the construction of the hybrid EM-circuit system matrix. In Section III, numerical results are presented. Both passive and active circuit devices are benchmarked. Conclusions are made at the end of this paper.

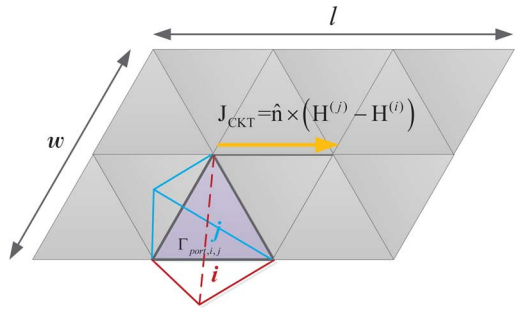

Fig. 1. Geometrical illustration of the boundary condition at the lumped port. $\hat{\mathbf{n}}$ is a unit normal vector pointing from element i to j.

II. Theory and Formulation

A. Formulation of DGTD

Suppose that we are concerning the EM field in the computational domain Ω bounded by $\partial\Omega$. The global domain Ω is meshed into a set of nonoverlapping subdomains Ω_i bounded by a surface $\partial\Omega_i$, where $\Omega=\bigcup\Omega_i$. Applying the discontinuous Galerkin testing procedure to the two first-order Maxwell's equations leads to the following two equations:

$$\int_{\Omega_i}\mathbf{\Phi}_k^{(i)}\cdot\left(\epsilon\frac{\partial\mathbf{E}}{\partial t}-\nabla\times\mathbf{H}+\mathbf{J}_{\rm im}\right)\,dV=\int_{\partial\Omega_i}\mathbf{\Phi}_k^{(i)}\cdot\left[\hat{\mathbf{n}}\times\left(\mathbf{H}^*-\mathbf{H}\right)\right]\,dS \tag{1}$$

$$\int_{\Omega_i}\mathbf{\Psi}_l^{(i)}\cdot\left(\mu\frac{\partial\mathbf{H}}{\partial t}+\nabla\times\mathbf{E}\right)\,dV=-\int_{\partial\Omega_i}\mathbf{\Psi}_l^{(i)}\cdot\left[\hat{\mathbf{n}}\times\left(\mathbf{E}^*-\mathbf{E}\right)\right]\,dS \tag{2}$$

where $\mathbf{\Phi}_k^{(i)}$ denotes the kth vector basis function for $\mathbf{E}$ in the ith subdomain and $\mathbf{\Psi}_l^{(i)}$ denotes the lth vector basis function for $\mathbf{H}$ in ith subdomain. $\mathbf{J}_{\rm im}$ is the externally imposed current density. $\hat{\mathbf{n}}$ is the unit outward normal vector of the ith subdomain. $\hat{\mathbf{n}}\times\mathbf{H}^*$ and $\hat{\mathbf{n}}\times\mathbf{E}^*$ are called the numerical flux for communications between adjacent elements. At the lumped port, a surface electric current density $\mathbf{J}_{\rm CKT}$ coupled from the circuit subsystem exists. The geometrical illustration is shown in Fig. 1. w and l represent the width and length of the rectangular lumped port, respectively. This surface port current density will impose a jump of the tangential magnetic field, which is incorporated into the numerical flux. By solving the Riemann problem with fulfilling the Rankine–Hugoniot condition, a general expression of the upwind flux can be derived as [20]–[23]

$$\hat{\mathbf{n}}\times\mathbf{H}^*=\hat{\mathbf{n}}\times\frac{\left(Z^{(i)}\mathbf{H}^{(i)}+\hat{\mathbf{n}}\times\mathbf{E}^{(i)}\right)+\left(Z^{(j)}\mathbf{H}^{(j)}-\hat{\mathbf{n}}\times\mathbf{E}^{(j)}\right)}{Z^{(i)}+Z^{(j)}}-\frac{Z^{(j)}\mathbf{J}_{\rm CKT}}{Z^{(i)}+Z^{(j)}} \tag{3}$$

$$\hat{\mathbf{n}} \times \mathbf{E}^* = \hat{\mathbf{n}} \times \frac{\left(Y^{(i)}\mathbf{E}^{(i)} - \hat{\mathbf{n}} \times \mathbf{H}^{(i)}\right) + \left(Y^{(j)}\mathbf{E}^{(j)} + \hat{\mathbf{n}} \times \mathbf{H}^{(j)}\right)}{Y^{(i)} + Y^{(j)}} - \frac{\mathbf{J}_{\mathrm{CKT}}}{Y^{(i)} + Y^{(j)}}. \tag{4}$$

The superscripts i and j represent local and its adjacent elements, respectively. $Z^{(i)} = \sqrt{\mu^{(i)}/\epsilon^{(i)}}$ is the intrinsic wave impedance in the ith element and $Z^{(j)} = \sqrt{\mu^{(j)}/\epsilon^{(j)}}$ is the intrinsic wave impedance in the corresponding neighboring element. $Y^{(i)} = 1/Z^{(i)}$ and $Y^{(j)} = 1/Z^{(j)}$ are intrinsic wave admittances. At boundary faces of elements with no lumped port, the extra term $\mathbf{J}_{\mathrm{CKT}}$ vanishes. The upwind flux based on the field tangential continuity condition is then recovered.

Next, fields $\mathbf{E}$ and $\mathbf{H}$ in the domain Ω_i are expanded by local basis functions $\mathbf{E} = \sum_{k=1}^{n_e^{(i)}} e_k^{(i)} \mathbf{\Phi}_k^{(i)}$, $\mathbf{H} = \sum_{l=1}^{n_h^{(i)}} h_l^{(i)} \mathbf{\Psi}_l^{(i)}$, where $n_e^{(i)}$ and $n_h^{(i)}$ are the number of degrees of freedom for $\mathbf{E}$ and $\mathbf{H}$ in the ith domain, respectively. $e_k^{(i)}$ and $h_k^{(i)}$ are time-dependent coefficients. By substituting these two expressions together with (3) and (4) into (1) and (2), the semi-discrete EM matrix system in elements where lumped ports reside can be constructed as

$$\mathbf{M}_e^{(i)} \frac{\partial \mathbf{e}^{(i)}}{\partial t} = \mathbf{S}_e^{(i)} \mathbf{h}^{(i)} - \mathbf{j}_{\mathrm{im}}^{(i)} - \mathbf{j}_e^{(i)} + \mathbf{F}_{ee}^{(ii)} \mathbf{e}^{(i)} - \mathbf{F}_{ee}^{(ij)} \mathbf{e}^{(j)} - \mathbf{F}_{eh}^{(ii)} \mathbf{h}^{(i)} + \mathbf{F}_{eh}^{(ij)} \mathbf{h}^{(j)} \tag{5}$$

$$\mathbf{M}_h^{(i)} \frac{\partial \mathbf{h}^{(i)}}{\partial t} = -\mathbf{S}_h^{(i)} \mathbf{e}^{(i)} + \mathbf{j}_h^{(i)} + \mathbf{F}_{hh}^{(ii)} \mathbf{h}^{(i)} - \mathbf{F}_{hh}^{(ij)} \mathbf{h}^{(j)} + \mathbf{F}_{he}^{(ii)} \mathbf{e}^{(i)} - \mathbf{F}_{he}^{(ij)} \mathbf{e}^{(j)} \tag{6}$$

where

$$\left[\mathbf{M}_e^{(i)}\right]_{(kl)} = \int_{\Omega_i} \mathbf{\Phi}_k^{(i)} \cdot \epsilon^{(i)} \mathbf{\Phi}_l^{(i)} \, dV \tag{7}$$

$$\left[\mathbf{M}_h^{(i)}\right]_{(kl)} = \int_{\Omega_i} \mathbf{\Psi}_k^{(i)} \cdot \mu^{(i)} \mathbf{\Psi}_l^{(i)} \, dV \tag{8}$$

$$\left[\mathbf{S}_e^{(i)}\right]_{(kl)} = \int_{\Omega_i} \mathbf{\Phi}_k^{(i)} \cdot \nabla \times \mathbf{\Psi}_l^{(i)} \, dV \tag{9}$$

$$\left[\mathbf{S}_h^{(i)}\right]_{(kl)} = \int_{\Omega_i} \mathbf{\Psi}_k^{(i)} \cdot \nabla \times \mathbf{\Phi}_l^{(i)} \, dV \tag{10}$$

$$\left[\mathbf{j}_{\mathrm{im}}^{(i)}\right]_{(k)} = \int_{\Omega_i} \mathbf{\Phi}_k^{(i)} \cdot \mathbf{J}_{\mathrm{im}}^{(i)} \, dV \tag{11}$$

$$\left[\mathbf{j}_e^{(ij)}\right]_{(k)} = \frac{Z^{(j)}}{Z^{(i)} + Z^{(j)}} \int_{\Gamma_{\mathrm{port},i,j}} \mathbf{\Phi}_k^{(i)} \cdot \mathbf{J}_{\mathrm{CKT}}^{(i)} \, dS \tag{12}$$

$$\left[\mathbf{j}_h^{(ij)}\right]_{(k)} = \frac{1}{Y^{(i)} + Y^{(j)}} \int_{\Gamma_{\mathrm{port},i,j}} \mathbf{\Psi}_k^{(i)} \cdot \hat{\mathbf{n}} \times \mathbf{J}_{\mathrm{CKT}}^{(i)} \, dS \tag{13}$$

$$\left[\mathbf{F}_{ee}^{(ii)}\right]_{(kl)} = \frac{1}{Z^{(i)} + Z^{(j)}} \int_{\partial\Omega_{i,j}} \mathbf{\Phi}_k^{(i)} \cdot \hat{\mathbf{n}} \times \left(\hat{\mathbf{n}} \times \mathbf{\Phi}_l^{(i)}\right) dS \tag{14}$$

$$\left[\mathbf{F}_{ee}^{(ij)}\right]_{(kl)} = \frac{1}{Z^{(i)} + Z^{(j)}} \int_{\partial\Omega_{i,j}} \mathbf{\Phi}_k^{(i)} \cdot \hat{\mathbf{n}} \times \left(\hat{\mathbf{n}} \times \mathbf{\Phi}_l^{(j)}\right) dS \tag{15}$$

$$\left[\mathbf{F}_{eh}^{(ii)}\right]_{(kl)} = \frac{Z^{(j)}}{Z^{(i)} + Z^{(j)}} \int_{\partial\Omega_{i,j}} \mathbf{\Phi}_k^{(i)} \cdot \hat{\mathbf{n}} \times \mathbf{\Psi}_l^{(i)} \, dS \tag{16}$$

$$\left[\mathbf{F}_{eh}^{(ij)}\right]_{(kl)} = \frac{Z^{(j)}}{Z^{(i)} + Z^{(j)}} \int_{\partial\Omega_{i,j}} \mathbf{\Phi}_k^{(i)} \cdot \hat{\mathbf{n}} \times \mathbf{\Psi}_l^{(j)} \, dS \tag{17}$$

$$\left[\mathbf{F}_{hh}^{(ii)}\right]_{(kl)} = \frac{1}{Y^{(i)} + Y^{(j)}} \int_{\partial\Omega_{i,j}} \mathbf{\Psi}_k^{(i)} \cdot \hat{\mathbf{n}} \times \left(\hat{\mathbf{n}} \times \mathbf{\Psi}_l^{(i)}\right) dS \tag{18}$$

$$\left[\mathbf{F}_{hh}^{(ij)}\right]_{(kl)} = \frac{1}{Y^{(i)} + Y^{(j)}} \int_{\partial\Omega_{i}} \mathbf{\Psi}_k^{(i)} \cdot \hat{\mathbf{n}} \times \left(\hat{\mathbf{n}} \times \mathbf{\Psi}_l^{(j)}\right) dS \tag{19}$$

$$\left[\mathbf{F}_{he}^{(ii)}\right]_{(kl)} = \frac{Y^{(j)}}{Y^{(i)} + Y^{(j)}} \int_{\partial\Omega_{i}} \mathbf{\Psi}_k^{(i)} \cdot \hat{\mathbf{n}} \times \mathbf{\Phi}_l^{(i)} \, dS \tag{20}$$

$$\left[\mathbf{F}_{he}^{(ij)}\right]_{(kl)} = \frac{Y^{(j)}}{Y^{(i)} + Y^{(j)}} \int_{\partial\Omega_{i,j}} \mathbf{\Psi}_k^{(i)} \cdot \hat{\mathbf{n}} \times \mathbf{\Phi}_l^{(j)} \, dS \tag{21}$$

where superscript $j \in N(i)$ ($N(i)$ is the set of indices of neighboring elements of element i). $\Gamma_{\mathrm{port},i,j}$ represents the lumped port surface shared by element i and j. $\mathbf{\Phi}_k^{(i)}$ and $\mathbf{\Psi}_k^{(i)}$ denote the kth testing basis for the $\mathbf{E}$ and $\mathbf{H}$-fields in the ith element, respectively. $\mathbf{\Phi}_l^{(j)}$ and $\mathbf{\Psi}_l^{(j)}$ denote the lth basis functions for the $\mathbf{E}$ and $\mathbf{H}$-fields in the jth element, respectively.

The first-order time derivatives in (5) and (6) will be approximated using the centering difference method with second-order accuracy, which is compatible with the circuit solver. The $\mathbf{E}$-field unknowns are evaluated at $t = n\delta t$ and the $\mathbf{H}$-field unknowns are evaluated at $t = (n + (1)/(2))\delta t$. To achieve a fully explicit time marching scheme, backward approximations $\mathbf{e}_{n+(1)/(2)}^{(i/j)} = \mathbf{e}_n^{(i/j)}$, $\mathbf{j}_{e,n+(1)/(2)}^{(i)} = (\mathbf{j}_{e,n+1}^{(i)} + \mathbf{j}_{e,n}^{(i)})/2$ in (7) and $\mathbf{h}_{n+1}^{(i/j)} = \mathbf{h}_{n+(1)/(2)}^{(i/j)}$ in (8) are applied for terms arising from the upwind flux.

In this way, the fully discrete local system equations can be obtained from the semi-discrete system in (5) and (6) as

$$\mathbf{M}_e^{(i)} \mathbf{e}_{n+1}^{(i)} + \delta t \frac{\mathbf{j}_{e,n+1}^{(i)}}{2} = \mathbf{M}_e^{(i)} \mathbf{e}_n^{(i)} + \delta t \left[\mathbf{S}_e^{(i)} \mathbf{h}_{n+\frac{1}{2}}^{(i)} - \mathbf{j}_{\mathrm{im},n+\frac{1}{2}}^{(i)} - \frac{\mathbf{j}_{e,n}^{(i)}}{2} + \mathbf{F}_{ee}^{(ii)} \mathbf{e}_n^{(i)} - \mathbf{F}_{ee}^{(ij)} \mathbf{e}_n^{(j)} - \mathbf{F}_{eh}^{(ii)} \mathbf{h}_{n+\frac{1}{2}}^{(i)} + \mathbf{F}_{eh}^{(ij)} \mathbf{h}_{n+\frac{1}{2}}^{(j)}\right] \tag{22}$$

$$\mathbf{M}_h^{(i)} \mathbf{h}_{n+\frac{3}{2}}^{(i)} = \mathbf{M}_h^{(i)} \mathbf{h}_{n+\frac{1}{2}}^{(i)} - \delta t \left[\mathbf{S}_h^{(i)} \mathbf{e}_{n+1}^{(i)} - \mathbf{j}_{h,n+1}^{(i)} - \mathbf{F}_{hh}^{(ii)} \mathbf{h}_{n+\frac{1}{2}}^{(i)} + \mathbf{F}_{hh}^{(ij)} \mathbf{h}_{n+\frac{1}{2}}^{(j)} - \mathbf{F}_{he}^{(ii)} \mathbf{e}_{n+1}^{(i)} + \mathbf{F}_{he}^{(ij)} \mathbf{e}_{n+1}^{(j)}\right]. \tag{23}$$

The unknown terms $\mathbf{E}_{n+1}^{(i)}$, $\mathbf{h}_{n+(3)/(2)}^{(i)}$, and $\mathbf{J}_{\mathrm{CKT},n+1}^{(i)}$ will be solved together with the following established circuit solver.

B. Circuit Equations Based on the Admittance Matrix in the Laplace Domain

The circuit equation system construction process is built upon the method in [4] based on the integral scheme. Suppose that an

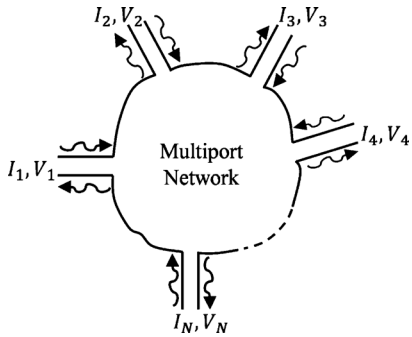

Fig. 2. Arbitrary circuit network with N ports. It can be characterized by the basic *I–V* relationship.

arbitrary lumped network has N ports, as shown in Fig. 2, and its basic *I–V* relationship in the Laplace domain is expressed as

$$\begin{bmatrix} i_1 \\ i_2 \\ \vdots \\ i_N \end{bmatrix} = \begin{bmatrix} \frac{Y_{11}^u(s^{-1})}{Y_{11}^d(s^{-1})} & \cdots & \frac{Y_{1N}^u(s^{-1})}{Y_{1N}^d(s^{-1})} \\ \vdots & \ddots & \vdots \\ \frac{Y_{N1}^u(s^{-1})}{Y_{N1}^d(s^{-1})} & \cdots & \frac{Y_{NN}^u(s^{-1})}{Y_{NN}^d(s^{-1})} \end{bmatrix} \begin{bmatrix} v_1 \\ v_2 \\ \vdots \\ v_N \end{bmatrix} \tag{24}$$

where i_i and v_i are port current and voltage in the Laplace domain, respectively. The matrix equation in (24) can be further transformed as follows:

$$\begin{bmatrix} d_1(s^{-1}) & \cdots & 0 \\ \vdots & \ddots & \vdots \\ 0 & \cdots & d_N(s^{-1}) \end{bmatrix} \begin{bmatrix} i_1 \\ i_2 \\ \vdots \\ i_N \end{bmatrix} = \begin{bmatrix} u_{11}(s^{-1}) & \cdots & u_{1N}(s^{-1}) \\ \vdots & \ddots & \vdots \\ u_{N1}(s^{-1}) & \cdots & u_{NN}(s^{-1}) \end{bmatrix} \begin{bmatrix} v_1 \\ v_2 \\ \vdots \\ v_N \end{bmatrix} \tag{25}$$

where

$$d_i(s^{-1}) = d_{i,0} + d_{i,1}s^{-1} + d_{i,2}s^{-2} + \cdots + d_{i,Q}s^{-Q} \tag{26}$$

denotes the lowest common multiple of

$$Y_{i1}^d(s^{-1}), \ldots, Y_{iN}^d(s^{-1}),$$

and

$$\begin{aligned} u_{ij}(s^{-1}) &= \frac{Y_{ij}^u(s^{-1})}{Y_{ij}^d(s^{-1})} \times d_i(s^{-1}) \\ &= u_{ij,0} + u_{ij,1}s^{-1} + u_{ij,2}s^{-2} + \cdots + u_{ij,P}s^{-P} \end{aligned} \tag{27}$$

where Q and P represent the orders of zeros and poles of the circuit network. $d_{i,q}$ and $u_{ij,p}$ denote the qth- and pth-order coefficients, respectively.

Next, the matrix equation in (25) is transformed from the Laplace domain to the time domain after some mathematical derivation. Namely,

$$\begin{aligned} &\begin{bmatrix} D_1(\delta t) & \cdots & 0 \\ \vdots & \ddots & \vdots \\ 0 & \cdots & D_N(\delta t) \end{bmatrix} \begin{bmatrix} I_1^{n+1} \\ I_2^{n+1} \\ \vdots \\ I_N^{n+1} \end{bmatrix} + \begin{bmatrix} \delta_1^n \\ \delta_2^n \\ \vdots \\ \delta_N^n \end{bmatrix} \\ &= \begin{bmatrix} U_{11}(\delta t) & \cdots & U_{1N}(\delta t) \\ \vdots & \ddots & \vdots \\ U_{N1}(\delta t) & \cdots & U_{NN}(\delta t) \end{bmatrix} \begin{bmatrix} V_1^{n+1} \\ V_2^{n+1} \\ \vdots \\ V_N^{n+1} \end{bmatrix} + \begin{bmatrix} \eta_1^n \\ \eta_2^n \\ \vdots \\ \eta_N^n \end{bmatrix} \end{aligned} \tag{28}$$

where

$$D_i(\delta t) = d_{i,0} + d_{i,1}\delta t + d_{i,2}(\delta t)^2 + \cdots + d_{i,Q}(\delta t)^Q \tag{29}$$

$$U_{ij}(\delta t) = u_{ij,0} + u_{ij,1}\delta t + u_{ij,2}(\delta t)^2 + \cdots + u_{ij,P}(\delta t)^P \tag{30}$$

$$\delta_i^n = [d_{i,1}, \ldots, d_{i,Q}] \left[\widetilde{I}_{i,1}^{n+1}, \ldots, \widetilde{I}_{i,Q}^{n+1}\right]^T \tag{31}$$

$$\eta_i^n = \sum_{j=1}^{N} \left([u_{ij,1}, \ldots, u_{ij,P}] \left[\widetilde{V}_{j,1}^{n+1}, \ldots, \widetilde{V}_{j,P}^{n+1}\right]^T \right) \tag{32}$$

$$\widetilde{I}_{i,q}^{n+1} = I_{i,q}^{n+1} - (\delta t)^q I_i^{n+1} \tag{33}$$

$$\widetilde{V}_{i,p}^{n+1} = V_{j,p}^{n+1} - (\delta t)^p V_j^{n+1} \tag{34}$$

$$\widetilde{I}_{i,0}^{n+1} = 0 \tag{35}$$

$$\widetilde{V}_{j,0}^{n+1} = 0 \tag{36}$$

$$I_{i,q}^{n+1} = (\delta t)^q \sum_{k_q=0}^{n} \cdots \sum_{k_2=0}^{k_3} \sum_{k_1=0}^{k_2} I_i^{k_1+1} \tag{37}$$

$$V_{j,p}^{n+1} = (\delta t)^p \sum_{k_p=0}^{n} \cdots \sum_{k_2=0}^{k_3} \sum_{k_1=0}^{k_2} V_j^{k_1+1} \tag{38}$$

$$I_{i,0}^{n+1} = I_i^{n+1} \tag{39}$$

$$V_{j,0}^{n+1} = V_j^{n+1}. \tag{40}$$

To efficiently calculate δ_i^n and η_j^n, two recursive updating schemes are developed in [4]. Namely,

$$\widetilde{I}_{i,q}^{n+1} = I_{i,q}^n + \delta t \cdot \widetilde{I}_{i,q-1}^{n+1} \tag{41}$$

$$\widetilde{V}_{j,p}^{n+1} = V_{j,p}^n + \delta t \cdot \widetilde{V}_{j,p-1}^{n+1}. \tag{42}$$

In this paper, another two necessary recursive relationships are derived apart from the above two. They are expressed as

$$I_{i,q}^n = I_{i,q}^{n-1} + \delta t \cdot I_{i,q-1}^n \tag{43}$$

$$V_{j,p}^n = V_{j,p}^{n-1} + \delta t \cdot V_{j,p-1}^n. \tag{44}$$

The dimension of the circuit matrix equation is $N^{\mathrm{CKT}} \times N^{\mathrm{CKT}}$ ($N = N^{\mathrm{CKT}}$). The unknowns involve the port current and voltage at $t = (n+1)\delta t$. After coupling this circuit matrix equation with the EM equations, the port voltage is derived from the line integral of the **E**-field along the lumped port surface.

C. Vector-Fitting Algorithm

There are situations that the circuit details are unknown or too complex to analytically calculate the admittance matrix, while only other network parameters such as S-parameters are available. In this case, the network parameters are firstly transformed to the admittance matrix based on the microwave network theory, then the fast-relaxation vector-fitting (FRVF) method [29]–[31] is used to approximate the admittance matrix elements. FRVF employs a rational function to approximate the sampled frequency admittance elements as

$$Y(s) = \sum_m \frac{c_m}{s - a_m} + d + se = \sum_m \frac{c_m s^{-1}}{1 - a_m s^{-1}} + d + \frac{e}{s^{-1}} \tag{45}$$

where c_m and a_m denote residues and poles, respectively. d and e are optional, and the variable $s = j\omega$. The vector-fitting technique includes two stages. The first stage is pole identification, and the second stage is residue identification. With this fitting method, our proposed algorithm is very flexible in the sense that we do not resort to specified circuit diagrams or analytical formulas for the lumped network as long as the frequency samples of its equivalent network parameters are available.

D. EM and Circuit Subsystems Coupling Scheme

We assume there are totally F independent lumped circuit networks and the EM domain is free of external current sources. Each of the circuit networks has K_f $(f = 1, 2, \ldots, F)$ ports. For the fth network, a rectangular lumped port is introduced at each interface between the EM region and this circuit network. Since the electrical size of the lumped port is small compared to the wavelength, quasi-static approximation is assumed with constant electric and magnetic fields over the lumped ports. Since there could be more than one element adjacent to the port q $(q = 1, 2, \ldots, K_f)$, we assume that the element i_q is one of the elements adjacent to the qth port. At the time $t = (n+1)\Delta t$, the supplied voltage at the qth lumped port can be calculated by the line integral of the $\mathbf{E}$ field in the i_q element along the lumped port. Namely,

$$\mathbf{V}^{\text{Port}}_{n+1,q,f} = -\sum_{k=1}^{n_e} e^{(i_q,f)}_{n+1,k,f} \int \mathbf{\Phi}^{(i_q,f)}_k \cdot \hat{l}_{q,f}\, dl = -[C]^{(i_q,f)}\{e\}^{(i_q,f)}_{n+1,f} \tag{46}$$

where $\hat{l}_{q,f}$ is the unit reference vector along the direction from the desired potential point to the reference potential point (reference ground) at the qth port. A schematic illustration of the coupling process is presented in Fig. 3. Since unknowns in the circuit subsystem are current $\mathbf{I}^{\text{CKT}}_p$ instead of current density $\mathbf{J}_{\text{CKT},p}$, (12) and (13) are reformulated

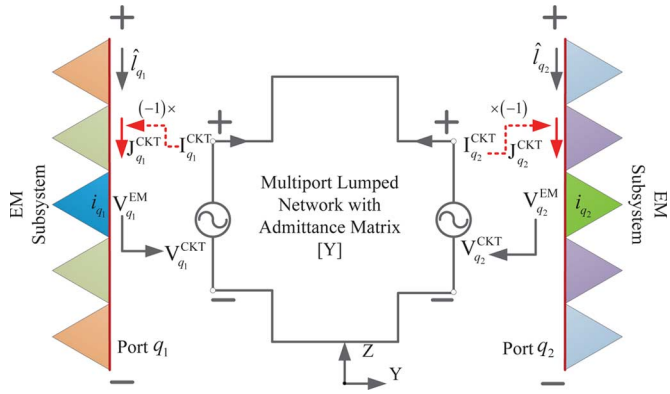

Fig. 3. (*side view*) Schematic illustration of the coupling between the EM subsystem (modeled by the DGTD) and the circuit subsystem (modeled by the admittance matrix in the Laplace domain). We assume that two of the rectangular lumped ports are parallel with the xz-plane, other ports are not shown for simplicity. Note that the reference direction of current flow in the EM domain and circuit network is opposite.

$$\left[\mathbf{j}^{(i_q,f)}_e\right]_{(n+1,q,k)} = \frac{Z^{(j)}\left(-\mathbf{I}^{\text{CKT}}_{n+1,q}\right)}{\left(Z^{(i_q,f)} + Z^{(j)}\right) w_{q,f}} \cdot \int_{\Gamma^q_{\text{port},i_q,f}} \mathbf{\Phi}^{(i_q,f)}_k \cdot \hat{l}_{q,f}\, dS = \mathbf{I}^{\text{CKT}}_{n+1,q,f}[\mathrm{T}_e]^{(i_q,f)}_{q,k} \tag{47}$$

$$\left[\mathbf{j}^{(i_q,f)}_h\right]_{(n+1,q,k)} = \frac{\left(-\mathbf{I}^{\text{CKT}}_{n+1,q}\right)}{\left(Y^{(i_q,f)} + Y^{(j)}\right) w_{q,f}} \int_{\Gamma^q_{\text{port},i_q,f}} \mathbf{\Psi}^{(i_q,f)}_k \cdot \hat{\mathbf{n}} \times \hat{l}_{q,f}\, dS = \mathbf{I}^{\text{CKT}}_{n+1,q,f}[\mathrm{T}_h]^{(i_q,f)}_{q,k}. \tag{48}$$

By combining (22), (28), (46), and (47), the locally coupled EM-circuit system equations can be established as

$$\mathbf{F}_f(\mathbf{x}_{n+1,f}) = \mathbf{b}^f_n \tag{49}$$

where

$$\mathbf{x}_{n+1,f} = \left\{ \left[\mathbf{e}^{(f)}_{n+1}\right]^{\mathrm{T}} \quad \left[\mathbf{V}^{\text{CKT}}_{n+1,f}\right]^{\mathrm{T}} \quad \left[\mathbf{I}^{\text{CKT}}_{n+1,f}\right]^{\mathrm{T}} \right\}^{\mathrm{T}} \tag{50}$$

$$\mathbf{e}^{(f)}_{n+1} = \left\{ \left[\mathbf{e}^{(i_1,f)}_{n+1}\right]^{\mathrm{T}}, \quad \left[\mathbf{e}^{(i_2,f)}_{n+1}\right]^{\mathrm{T}}, \quad \ldots \quad \left[\mathbf{e}^{(i_{K_f},f)}_{n+1}\right]^{\mathrm{T}} \right\}^{\mathrm{T}} \tag{51}$$

$\mathbf{V}^{\text{CKT}}_{n+1,f}$ is comprised of lumped port voltages. $\mathbf{I}^{\text{CKT}}_{n+1,f}$ contains the amplitude of currents through lumped ports

$$\mathbf{F}_f(\mathbf{x}_{n+1,f}) = \begin{bmatrix} [\mathbf{M}^f_e] & \mathbf{0} & \delta t\,[\mathbf{T}^f_e/2] \\ \mathbf{0} & -[\mathbf{U}^f] & [\mathbf{D}^f] \\ [\mathbf{C}^f] & -[\mathbf{I}^f] & \mathbf{0} \end{bmatrix} \begin{bmatrix} \mathbf{e}^{(f)}_{n+1} \\ \mathbf{V}^{\text{CKT}}_{n+1,f} \\ \mathbf{I}^{\text{CKT}}_{n+1,f} \end{bmatrix} \tag{52}$$

$$\mathbf{b}_n^f = \begin{bmatrix} \mathbf{b}_{\mathrm{EM}}^f \\ \boldsymbol{\eta}_n^f - \boldsymbol{\delta}_n^f \\ \mathbf{0} \end{bmatrix} \tag{53}$$

with $[\mathbf{M}_e^f]$, $[\mathbf{T}_e^f]$ and $[\mathbf{C}^f]$ are diagonal matrices, and $[\mathbf{I}^f]$ is an identity matrix. $\mathbf{b}_{\mathrm{EM}}^f$, $\boldsymbol{\eta}_{n,f}$, and $\boldsymbol{\delta}_{n,f}$ are column vectors. Namely,

$$\left[\mathbf{M}_e^f\right]_{\mathrm{diag}} = \left[\mathbf{M}_e^{(i_1,f)},\ \mathbf{M}_e^{(i_2,f)},\ \cdots,\ \mathbf{M}_e^{(i_{K_f},f)}\right] \tag{54}$$

$$\left[\mathbf{T}_e^f\right]_{\mathrm{diag}} = \left[\mathbf{T}_e^{(i_1,f)},\ \mathbf{T}_e^{(i_2,f)},\ \cdots,\ \mathbf{T}_e^{(i_{K_f},f)}\right] \tag{55}$$

$$\left[\mathbf{C}^f\right]_{\mathrm{diag}} = \left[\mathbf{C}^{(i_1,f)},\ \mathbf{C}^{(i_2,f)},\ \cdots,\ \mathbf{C}^{(i_{K_f},f)}\right] \tag{56}$$

$$\begin{aligned} \mathbf{b}_{\mathrm{EM}}^{i_q,f} &= \mathbf{M}_e^{(i_q,f)}[\mathbf{e}_n]^{(i_q,f)} \\ &\quad + \Delta t \left[\mathbf{S}_e^{(i_q,f)}\mathbf{h}_{n+\frac{1}{2}}^{(i)} - \frac{\mathbf{I}_{n,q,f}^{\mathrm{CKT}}[\mathbf{T}_e]^{(i_q,f)}}{2}\right. \\ &\quad + \mathbf{F}_{ee}^{(i_q i_q)}\mathbf{e}_n^{(i_q,f)} - \mathbf{F}_{ee}^{(i_q j)}\mathbf{e}_n^{(j)} \\ &\quad \left. -\mathbf{F}_{eh}^{(i_q i_q)}\mathbf{h}_{n+\frac{1}{2}}^{(i_q,f)} + \mathbf{F}_{eh}^{(i_q j)}\mathbf{h}_{n+\frac{1}{2}}^{(j)}\right]. \end{aligned} \tag{57}$$

The overall dimension of the coupled matrix in (52) is equal to $n_e^{(i_1,f)}+n_e^{(i_2,f)}+\cdots+n_e^{(i_{K_f},f)}+N_f^{\mathrm{CKT}}$. In this paper, the EM domain is split into tetrahedron. Each mesh cell is assigned six edge vector basis functions. Hence, only a square matrix with the dimension equal to $6K_f + N_f^{\mathrm{CKT}}$ needs to be inverted.

E. Stability and LTS

The resultant marching scheme is explicit and conditionally stable. For the stability condition, the time-stepping size for the ith element is chosen in terms of the following condition [16], [17], [24] derived by energy conversation technique:

$$c_i \delta t_i \left[\frac{4\sqrt{5}}{3} + \frac{8}{3}\max\left(\sqrt{\frac{\mu_i}{\mu_j}}, \sqrt{\frac{\epsilon_i}{\epsilon_j}}\right)\right] < \frac{4V_i}{P_i} \tag{58}$$

where $j \in N(i)$ represents the set of neighboring elements of the ith element, $c_i = (1)/(\sqrt{\epsilon_i \mu_i})$ is the speed of light, P_i is the total area of four facets, and V_i is the volume of element i. The ratio of $(4V_i)/(P_i)$ effectively represents the diameter h_i of the finite element. As the ratio of $(4V_i)/(P_i)$ becomes smaller, the time-stepping size will also reduce, which will increase the computational time significantly. To improve the efficiency of this hybrid EM-circuit simulation algorithm, the LTS method developed in [25] is employed to handle the generated unstructured meshes in practical applications. This strategy regroups the elements according to the local time-step size. For the kth group, its time-step size is $\delta t_k = (2m+1)^{k-1}\delta t_{\min}$ with $\delta t_{\min} = \min(\delta t_i)$ denoting the minimum global time-stepping size. In our case, $m = 1$ is chosen, which means that there is a factor of 3 between the time steps of consecutive classes. For mesh cells that are not located at the interface between different groups, the classical leapfrog is applied. Otherwise, the terms coming from the neighboring elements acquire the recently updated field values from the corresponding adjacent elements.

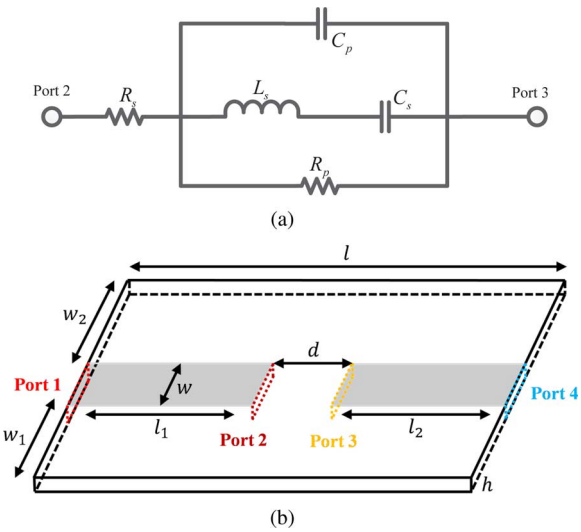

Fig. 4. (a) Equivalent circuit of the chip capacitor. (b) Layout of the circuit configuration. $l = 2.5$ mm, $l_1 = 1$ mm, $l_2 = 1$ mm, $w = 0.79$ mm, $w_1 = 1.105$ mm, $w_2 = 1.105$ mm, $d = 0.5$ mm, $h = 0.254$ mm, $L_s = 0.02$ nH, $C_p = 5.07$ pF, $C_s = 14.93$ pF, $R_p = 268\ \Omega$, $R_s = 0.139\ \Omega$.

TABLE I
ELEMENT PARTITIONING BY CLASSES FOR THE CHIP CAPACITOR

*Class	*Elements	$*\delta t(s)$
1	64	8.55e-15
2	3935	2.565e-14
3	1796	7.695e-14

III. NUMERICAL RESULTS

In this section, several numerical examples are benchmarked to valid the feasibility and accuracy of the proposed algorithm. Both passive and active devices are included. To truncate the computational domain, first-order absorbing absorbing boundary conditions are employed [16], [20].

A. Chip Capacitor

To verify the feasibility of our method, a microstrip interconnect structure shown in Fig. 4(a) and a Gap-Cap chip capacitor G15BU200K5PX05 [3] represented by the equivalent circuit shown in Fig. 4(b) is studied by the proposed algorithm. The substrate height is 0.254 mm, and the relative dielectric constant is 2.17. The mesh elements are classified into three groups. The number of elements and time-step size for each class are presented in Table I. The admittance matrix for this circuit network is analytically derived and formulated as

$$\begin{aligned} Y_{11} &= \frac{s^{-3} + a_1 s^{-2} + a_2 s^{-1} + a_3}{b_0 s^{-3} + b_1 s^{-2} + b_2 s^{-1} + b_3} \\ Y_{12} &= -Y_{11} \\ Y_{21} &= -Y_{11} \\ Y_{22} &= Y_{11} \end{aligned} \tag{59}$$

where $a_1 = (C_p + C_s)R_p$, $a_2 = L_s C_s$, $a_3 = R_p L_s C_s C_p$, $b_0 = R_s + R_p$, $b_1 = a_1 R_s$, $b_2 = a_2(R_s + R_p)$, and $b_3 = a_3 R_s$.

To characterize the attenuation effects of this capacitor, a differential Gaussian pulse Thevenin voltage source [27] is applied at port 1. The CPU time for 307 200 time steps based on the minimum time step size is shown in Table II. The computational

TABLE II
CPU GAIN TIME OF LTS VERSUS THE STANDARD LEAPFROG SCHEME

CPU time with LTS	9.52 min
CPU time without LTS	37.03 min
CPU gain with LTS	3.89

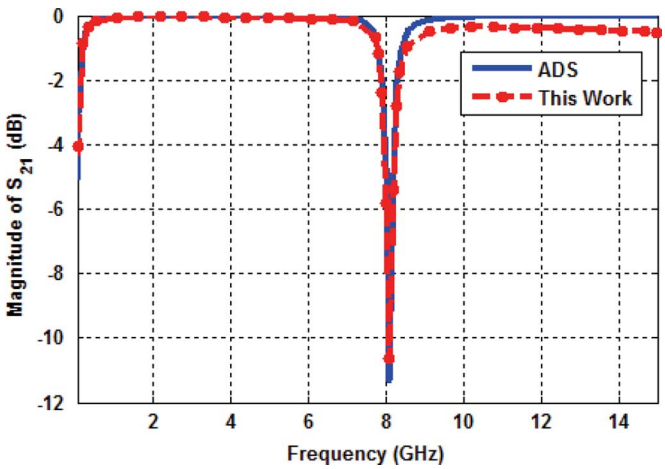

Fig. 5. Magnitude of S_{11} and S_{21} calculated by the proposed algorithm and reference from ADS simulation [32].

gain of LTS is 3.89. Fig. 5 shows the calculated transmission coefficient S_{21}. It is noted that there is a deep null around 8 GHz. For comparison, the result from ADS [32] is also presented. Good agreements are observed. Our result also complies with the result calculated by TP-LN-FDTD method in [3].

B. Small-Signal Model of MESFET

To further demonstrate the proposed algorithm is capable of modeling active devices, a microwave metal–semiconductor–field-effect transistor (MESFET) amplifier is simulated. Both the intrinsic and extrinsic equivalent circuit model of the MESFET are considered.

1) Intrinsic Equivalent-Circuit Model of MESFET: The intrinsic part of its small-signal equivalent circuit is shown in Fig. 6(a). The substrate and the microstrip line matching networks are the same as that in Fig. 4(b). Hence, the same mesh structure in Section III-A is utilized. For the intrinsic part, the gate terminal G' and the drain terminal D' are connected to ports 2 and 3, respectively. The admittance parameters of this circuit are analytically derived as

$$\begin{aligned} Y_{11} &= \frac{(C_{\rm gs}+C_{\rm gd})s^{-1}+C_{\rm gd}C_{\rm gs}R_i}{s^{-2}+C_{\rm gs}R_i s^{-1}} \\ Y_{12} &= -C_{\rm gd}/s^{-1} \\ Y_{21} &= \frac{G_m s^{-2}-C_{\rm gd}s^{-1}-C_{\rm gd}C_{\rm gs}R_i}{s^{-2}+C_{\rm gs}Rs^{-1}} \\ Y_{22} &= G_{\rm ds}+(C_{\rm ds}+C_{\rm gd})/s^{-1}. \end{aligned} \tag{60}$$

The broadband frequency-domain characteristics is investigated by applying a Gaussian voltage source at port 1. The transient voltages at Port 1 and Port 4 simulated by the LTS scheme

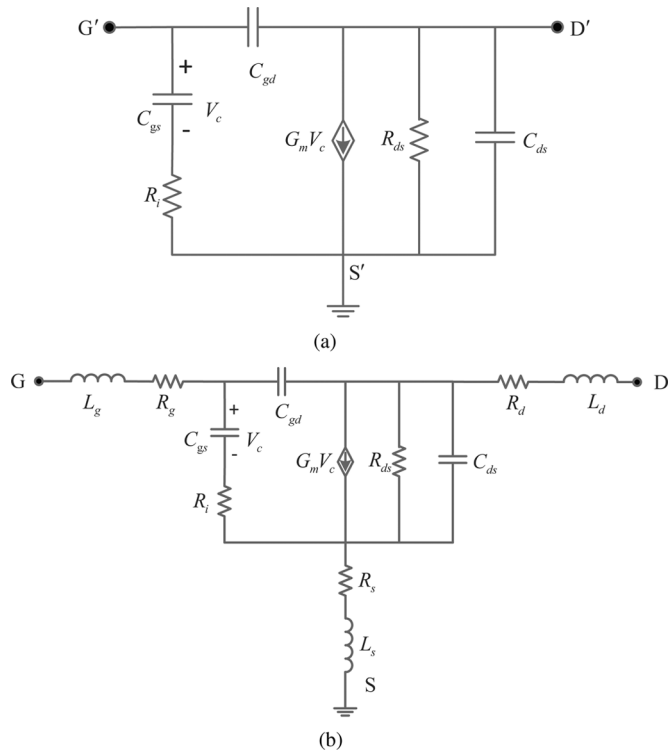

Fig. 6. (a) Intrinsic equivalent circuit of the small-signal MESFET. (b) Extrinsic equivalent circuit of the small-signal MESFET. $L_g = 0.37$ nH, $L_d = 0.23$ nH, $L_s = 0.02$ nH, $C_{\rm gd} = 0.06$ pF, $C_{\rm ds} = 0.26$ pF, $C_{\rm gs} = 0.69$ pF, $R_g = 1.39\ \Omega$, $R_s = 0.76\ \Omega$, $R_i = 1.42\ \Omega$, $R_{\rm ds} = 197\ \Omega$, $R_d = 1.3\ \Omega$, and $G_m = 65$ mS.

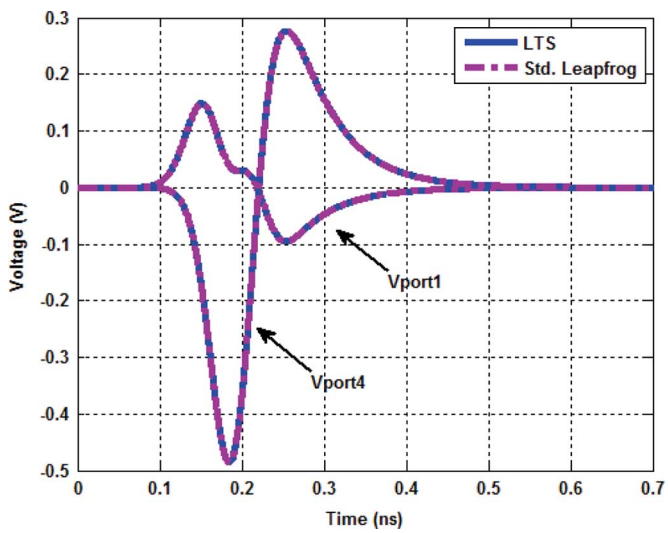

Fig. 7. Simulated voltages at ports 1 and 4 versus the time sequence.

and standard leapfrog method are shown in Fig. 7. Good agreements are observed, which means the LTS scheme will not deteriorate the accuracy compared with those from the standard leapfrog technique. Fig. 8 describes the simulated S-parameters. Also, reasonable agreements between the proposed algorithm and ADS are noted. The difference between the proposed solver and ADS might be due to the lack of full-wave ability of

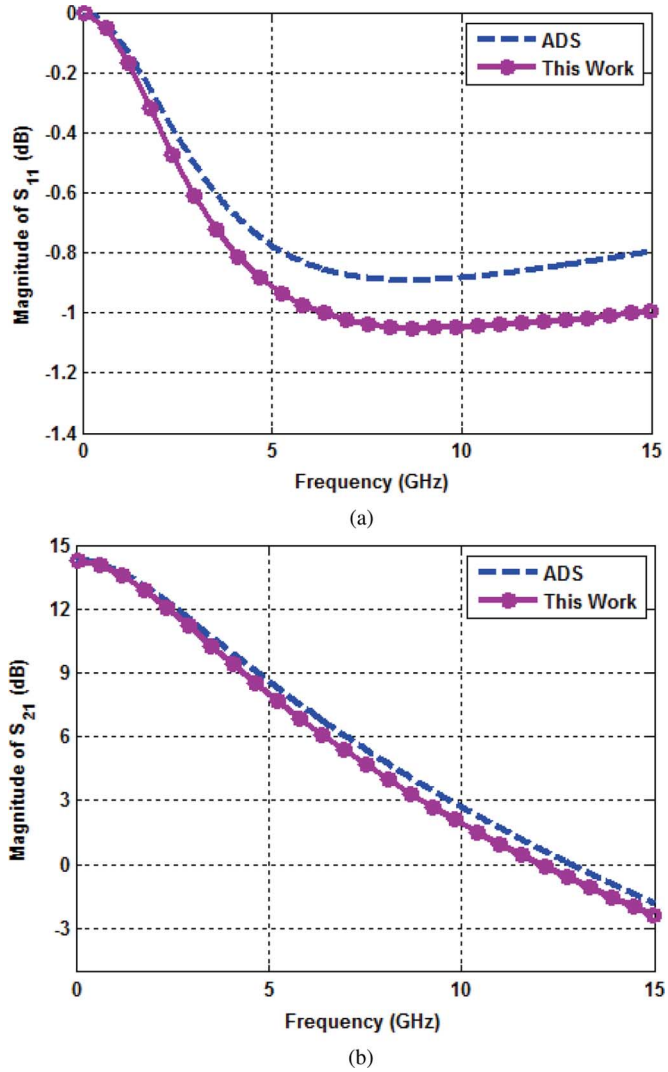

Fig. 8. Magnitude of: (a) S_{11} and (b) S_{21} for the intrinsic MESFET amplifier circuit.

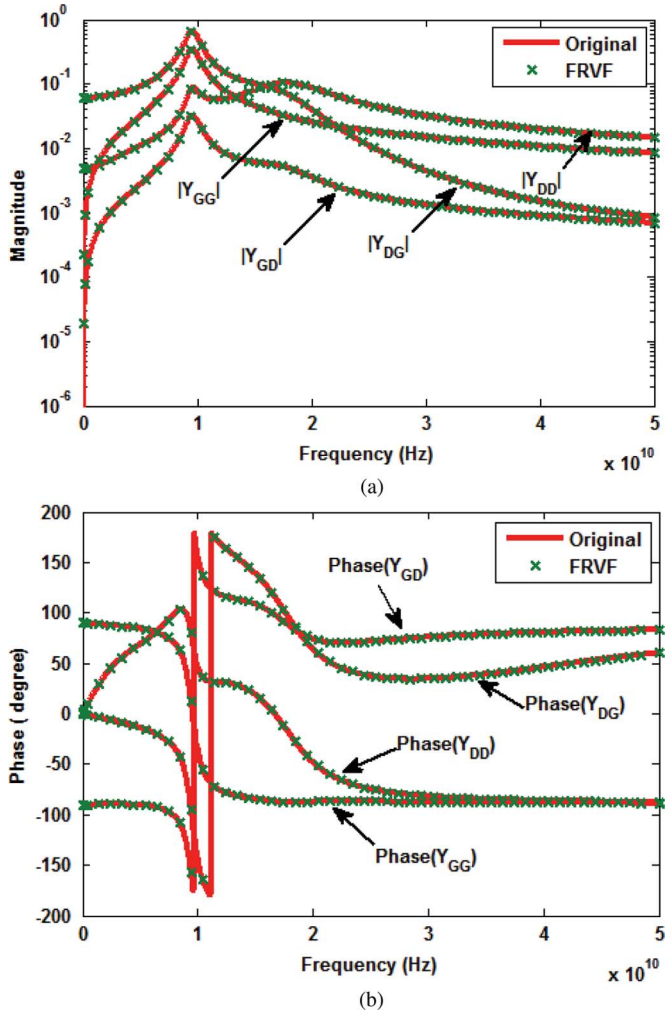

Fig. 9. (a) Magnitude of the original and fitted admittance values. (b) Phase of the original and fitted admittance values.

ADS. In fact, the simulated results have good agreements with those by the FDTD [3].

2) Extrinsic Equivalent-Circuit Model of MESFET: To incorporate the general model of the MESFET devices, the parasitic parameters at the gate, drain, and source terminals are included in the equivalent-circuit model. This model is called the extrinsic model [3], [13], [28], as shown in Fig. 6(b). The gate G and drain D are connected to ports 2 and 3, respectively. To analytically derive the admittance matrix of this circuit, it is quite difficult and time consuming. Alternately, the FRVF method discussion in Section II is used to approximate the admittance matrix elements by rational functions.

In our case, $e = 0$ is chosen. The S-parameters of the extrinsic network from dc to 50 GHz are obtained by ADS simulation with a 50-MHz frequency step. The frequency-domain admittance matrix Y is transformed from S-parameters according to the microwave network theory. In this example, the number of poles is equal to 4. The coefficients a, c, d of the fitted admittance parameters are listed in the Appendix. Fig. 9 shows the fitted admittance values including both magnitude and phase. It is clearly noted that excellent agreements with the sampled data are achieved.

TABLE III
CPU GAIN WITH LTS VERSUS THE STANDARD LEAPFROG SCHEME

CPU time with LTS	3.69 min
CPU time without LTS	14.01 min
CPU gain with LTS	3.80

With these fitted admittance values, this extrinsic model can be integrated with the proposed algorithm. By applying a differential Gaussian voltage source at port 1, the broadband properties can be easily characterized. The CPU time for 101 376 time steps based on the minimum time step size is presented in Table III. The CPU gain of the LTS over the standard leapfrog method is 3.80. The simulated S-parameters are shown in Fig. 10. Results from ADS are also presented for comparison. The difference from the ADS is due to the lack of full-wave capability of ADS simulations. For full-wave comparison, our results agree very well with those from the TDFEM in [13].

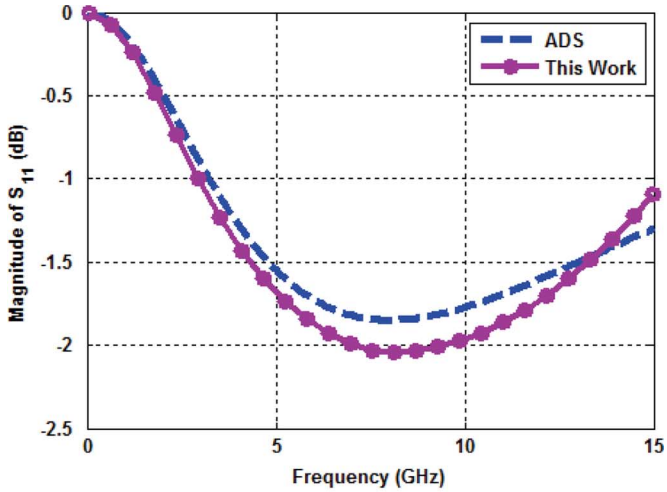

(a)

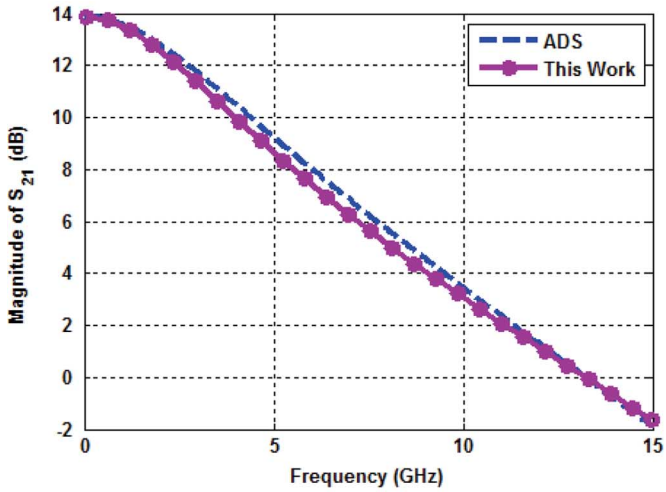

(b)

Fig. 10. Magnitude of: (a) S_{11} and (b) S_{21} for the extrinsic MESFET amplifier circuit.

IV. Conclusion

In this paper, a hybrid full-wave EM-circuit simulator based on the DGTD and admittance matrix is developed to simulate circuit systems. The coupling between the EM solver with the circuit solver is realized by introducing an external voltage source and current at the lumped port. Due to the local operations of the DGTD, only small coupling matrix equations are involved. To increase the efficiency of the time-marching scheme, the LTS strategy is employed to dynamically facilitate the time marching on the element level. For validation purposes, multiport lumped networks including both passive *R*, *L*, and *C* networks and active microwave MESFET amplifiers are analyzed. For cases that circuit details are unavailable or too complex to derive the mathematical expressions of admittance matrix elements, the FRVF method is employed to obtain the approximated admittance matrix as long as frequency samples of its S-parameters are known. It further maximizes the proposed method's flexibility.

TABLE IV
Value of Coefficient a_{ij} ($\times 10^{12}$) for the Admittance Elements

nm	$a_{nm,1}$	$a_{nm,2}$	$a_{nm,3}$	$a_{nm,4}$
Y_{11}	-0.381+j6.011	$a^*_{11,1}$	-2.089+j11.094	$a^*_{11,3}$
Y_{12}	-0.381+j6.011	$a^*_{12,1}$	-2.089+j11.094	$a^*_{12,3}$
Y_{21}	-0.381+j6.011	$a^*_{21,1}$	-2.089+j11.094	$a^*_{21,3}$
Y_{22}	-0.381+j6.011	$a^*_{22,1}$	-2.089+j11.094	$a^*_{22,3}$

TABLE V
Value of Coefficient c_{ij} ($\times 10^{9}$) for the Admittance Elements

nm	$c_{nm,1}$	$c_{nm,2}$	$c_{nm,3}$	$c_{nm,4}$
Y_{11}	1.318+j0.0702	$c^*_{11,1}$	-0.0307+j0.0195	$c^*_{11,3}$
Y_{12}	-0.119+j0.0315	$c^*_{12,1}$	0.016+j0.0487	$c^*_{12,3}$
Y_{21}	-0.799+j2.524	$c^*_{21,1}$	0.596+j1.31	$c^*_{21,3}$
Y_{22}	0.016+j0.244	$c^*_{22,1}$	1.993+j0.362	$c^*_{22,3}$

Appendix

The circuit matrix equation for the extrinsic equivalent circuit of the small-signal field-effect transistor (FET) can be formulated as

$$\begin{bmatrix} i_1 \\ i_2 \end{bmatrix} = \begin{bmatrix} Y_{11}(s^{-1}) & Y_{12}(s^{-1}) \\ Y_{21}(s^{-1}) & Y_{22}(s^{-1}) \end{bmatrix} \begin{bmatrix} v_1 \\ v_2 \end{bmatrix} \tag{61}$$

where the element $Y_{i,j}(s^{-1})$ $(i,\ j = 1, \ldots, 4)$ is obtained by FRVT using a rational function, and expressed as

$$Y_{ij} = \frac{c_{ij,1}s^{-1}}{1 - a_{ij,1}s^{-1}} + \frac{c_{ij,2}s^{-1}}{1 - a_{ij,2}s^{-1}} + \frac{c_{ij,3}s^{-1}}{1 - a_{ij,3}s^{-1}} + \frac{c_{ij,4}s^{-1}}{1 - a_{ij,4}s^{-1}} + d_{ij} \tag{62}$$

where the coefficients a_{ij}, c_{ij}, and d_{ij} are determined via the two stages discussed in the vector fitting part.

In Tables IV and V, the coefficients a_{ij} and c_{ij} for Y_{11}, Y_{12}, Y_{21}, and Y_{22} are presented. The superscript * denotes the complex conjugate. The coefficient d_{ij} are $d_{11} = -3.309 \times 10^{-8}$, $d_{12} = -7.1551 \times 10^{-9}$, $d_{21} = -7.1057 \times 10^{-9}$, and $d_{22} = -1.5365 \times 10^{-9}$.

Acknowledgment

The authors are grateful for the constructive suggestions from Prof. W. C. Chew.

References

[1] A. Vladimirescu, *The Spice Book*. New York, NY, USA: Wiley, 1994.
[2] J. A. Pereda, F. Alimenti, P. Mezzanotte, L. Roselli, and R. Sorrentino, "A new algorithm for the incorporation of arbitrary linear lumped networks into FDTD simulators," *IEEE Trans. Microw. Theory Techn.*, vol. 47, no. 6, pp. 943–949, Jun. 1999.
[3] O. Gonzalez, J. A. Pereda, A. Herrera, and A. Vegas, "An extension of the lumped-network FDTD method to linear two-port lumped circuits," *IEEE Trans. Microw. Theory Techn.*, vol. 54, no. 7, pp. 3045–3051, Jul. 2006.
[4] C. C. Wang and C. W. Kuo, "An efficient scheme for processing arbitrary lumped multiport devices in the finite-difference time-domain method," *IEEE Trans. Microw. Theory Techn.*, vol. 55, no. 5, pp. 958–965, May 2007.

[5] M. Piket-May, A. Taflove, and J. Baron, "FD-TD modeling of digital signal propagation in 3-D circuits with passive and active loads," *IEEE Trans. Microw. Theory Techn.*, vol. 42, no. 8, pp. 1514–1523, Aug. 1994.
[6] W. Sui, D. A. Christensen, and C. H. Durney, "Extending the two-dimensional FDTD method to hybrid electromagnetic systems with active and passive lumped elements," *IEEE Trans. Microw. Theory Techn.*, vol. 40, no. 4, pp. 724–730, Apr. 1992.
[7] C. N. Kuo, B. Houshmand, and T. Itoh, "FDTD analysis of active circuits with equivalent current source approach," in *IEEE AP-S Int. Symp. Dig.*, Jun. 1995, vol. 3, pp. 1510–1513.
[8] C. N. Kuo, R. B. Wu, B. Houshmand, and T. Itoh, "Modeling of microwave active devices using FDTD analysis based on the voltage source approach," *IEEE Trans. Microw. Guided Wave Lett.*, vol. 6, no. 5, pp. 199–201, May 1996.
[9] K. P. Ma, M. Vhen, B. Houshband, Y. Qian, and T. Itoh, "Global time-domain full-wave analysis of microwave circuits involving highly nonlinear phenomena and EMC effects," *IEEE Trans. Microw. Theory Techn.*, vol. 47, no. 6, pp. 859–866, Jun. 1999.
[10] A. Taflove, *Computational Electrodynamics: The Finite-Difference Time-Domain Method*. Norwood, MA, USA: Artech House, 1995.
[11] J. M. Jin, *The Finite Element Method in Electromagnetics*, 2nd ed. New York, NY, USA: Wiley, 2003.
[12] R. Wang and J. M. Jin, "A symmetric electromagnetic-circuit simulator based on the extended time-domain finite lement method," *IEEE Trans. Microw. Theory Techn.*, vol. 56, no. 12, pp. 2875–2884, Dec. 2008.
[13] R. Wang and J. M. Jin, "Incorporation of multiport lumped networks into the hybrid time-domain finite-element analysis," *IEEE Trans. Microw. Theory Techn.*, vol. 57, no. 8, pp. 2030–2037, Aug. 2009.
[14] Q. He and D. Jiao, "Fast electromagnetic-based co-simulation of linear network and nonlinear circuits for the analysis of high-speed integrated circuits," *IEEE Trans. Microw. Theory Techn.*, vol. 58, no. 12, pp. 3677–3687, Dec. 2010.
[15] X. Li and J. M. Jin, "A comparative study of three finite element-based explicit numerical schemes for solving Maxwell's equations," *IEEE Trans. Antennas Propag.*, vol. 60, no. 3, pp. 1450–1457, Mar. 2012.
[16] S. Dosopoulos and J. F. Lee, "Interconnect and lumped elements modeling in interior penalty discontinuous Galerkin time-domain methods," *J. Comput. Phys.*, vol. 229, pp. 8521–8536, Aug. 2010.
[17] S. Dosopoulos, B. Zhao, and J. F. Lee, "Non-conformal and parallel discontinuous Galerkin time domain method for Maxwell's equations: EM analysis of IC packages," *J. Comput. Phys.*, vol. 238, pp. 48–70, Dec. 2012.
[18] B. Zhao, J. C. Yong, and S. D. Gedney, "SPICE lumped circuit subcell model for the discontinuous Galerkin finite element time-domain method," *IEEE Trans. Microw. Theory Techn.*, vol. 60, no. 9, pp. 2648–2692, Sep. 2012.
[19] P. Li and L. J. Jiang, "A hybrid electromagnetics-circuit simulation method exploiting discontinuous Galerkin finite element time domain method," *IEEE Microw. Wireless Compon. Lett.*, vol. 23, no. 3, pp. 113–115, Mar. 2013.
[20] J. Alvarez, L. D. Angulo, M. F. Pantoja, A. R. Bretones, and S. G. Garcia, "Source and boundary implementation in vector and scalar DGTD," *IEEE Trans. Antennas Propag.*, vol. 58, no. 6, pp. 1997–2003, Jun. 2010.
[21] J. Alvarez, L. D. Angulo, A. R. Bretones, and S. G. Garcia, "A spurious-free discontinuous Galerkin time domain for the accurate modeling of microwave filters," *IEEE Trans. Microw. Theory Techn.*, vol. 60, no. 8, pp. 2359–2369, Aug. 2012.
[22] J. Alvarez, L. D. Angulo, A. R. Bretones, C. de Jong, and S. G. Garcia, "3D discontinuous Galerkin time domain method for anisotropic materials," *IEEE Antennas Wireless Propag. Lett.*, vol. 11, pp. 1182–1185, 2012.
[23] K. Sankaran, "Accurate domian truncation techniques for time-domain conformal methods," Ph.D. dissertation, Dept. Inform. Technol. Elect. Eng., ETH Zurich, Zurich, Switzerland, 2007.
[24] L. Fezoui, S. Lanteri, S. Lohrengel, and S. Piperno, "Convergence and stability of a discontinuous Galerkin time-domain method for the 3-D heterogeneous Maxwell equations on unstructured meshes," *ESAIM: M2AN*, vol. 39, no. 6, pp. 1149–1176, 2005.
[25] E. Montseny, S. Pernet, X. Ferrieres, and G. Cohen, "Dissipative terms and local time-stepping imrpovements in a spatial high order discontinuous Galerkin scheme for the time-domian method for the time-domain Maxwell's equations," *J. Comput. Phys.*, vol. 227, no. 14, pp. 6795–6820, Apr. 2008.
[26] R. Wang and J. M. Jin, "A flexible time-stepping scheme for hybrid field-circuit simulation based on the extended time-domain finite element method," *IEEE Trans. Adv. Packag.*, vol. 33, no. 3, pp. 769–776, Mar. 2010.
[27] O. P. M. Pekonen and J. Xu, "Rigorous analysis of circuit parameter extraction from an FDTD simulation excited with a resistive voltage source," *Microw. Opt. Technol.*, vol. 12, no. 4, pp. 205–210, Jul. 1996.
[28] Z. Zheng, "Novel modelling methods for microwave GaAs MESFET device," Ph.D. dissertation, Dept. Elect. Comput. Eng., Nat. Univ. Singapore, Singapore, Singapore, 2010.
[29] B. Gustavsen and A. Semlyen, "Rational approximation of frequency domian responses by vector fitting," *IEEE Trans. Power Del.*, vol. 14, no. 3, pp. 1052–1061, Jul. 1999.
[30] B. Gustavsen, "Improving the pole relocating properties of vector fitting," *IEEE Trans. Power Del.*, vol. 21, no. 3, pp. 1587–1592, Jul. 2006.
[31] D. Deschrijver, M. Mrozowski, T. Dhaene, and D. D. Zutter, "Macromodeling of multiport systems using a fast implementation of the vector fitting method," *IEEE Microw. Wireless Compon. Lett.*, vol. 18, no. 6, pp. 383–385, Jun. 2008.
[32] Adv. Design Syst. (ADS). Agilent Technol., Santa Clara, CA, USA, 2012. [Online]. Available: http://eesof.tm.agilent.com/products/
[33] C. Ho, A. E. Ruehli, and P. A. Brennan, "The modified nodal approach to newtork analysis," *IEEE Trans. Circuits Syst.*, vol. CAS-22, no. 6, pp. 504–509, Jun. 1975.

Ping Li (S'12) received the Bachelor's and Master's degree from the University of Electronic Science and Technology of China, Chendu, China, in 2008 and 2010, respectively, and is currently working toward the Ph.D. degree at the University of Hong Kong, Hong Kong.

From September 2008 to August 2010, he was with the University of Electronic Science and Technology of China. Since 2010, he has been with the Center of Electromagnetics and Optics, University of Hong Kong. His research interests include the inverse scattering/radiation problem, the time-domain discontinuous Galerkin FEM and its application in microwave wave-device simulation, and nanophotonics analysis.

Mr. Li was the recipient of the Engineering Postgraduate Fellowship of the Faculty of Engineering, University of Hong Kong.

Li Jun Jiang (S'01–M'04–SM'13) received the B.S. degree in electrical engineering from the Beijing University of Aeronautics and Astronautics, Beijing, China, in 1993, the M.S. degree from the Tsinghua University, Beijing, China, in 1996, and the Ph.D. from the University of Illinois at Urbana-Champaign, Urbana, IL, USA, in 2004.

From 1996 to 1999, he was an Application Engineer with the Hewlett-Packard Company. Since 2004, he has been a Postdoctoral Researcher, Research Staff Member, and Senior Engineer with the IBM T. J. Watson Research Center. Since the end of 2009, he has also been an Associate Professor with the Department of Electrical and Electronic Engineering, University of Hong Kong, Hong Kong. His research interests focus on electromagnetics, integrated circuit (IC) signal/power integrity, antennas, multidisciplinary electronic design automation (EDA) solutions, RF and microwave technologies, and high-performance computing (HPC).

Dr. Jiang is a member of the IEEE Antennas and Propagation Society (AP-S). He is an Associate Member of Sigma Xi. He was the Semiconductor Research Cooperation (SRC) industrial liaison for several academic projects. Since 2009, he has been the SRC packaging high-frequency tel-topic (TT) chair. He serves as a reviewer for IEEE TRANSACTIONS on several topics and other primary electromagnetics- and microwave-related journals. He was the recipient of the IEEE Microwave Theory and Techniques Society (IEEE MTT-S) Graduate Fellowship Award in 2003 and the Y. T. Lo Outstanding Research Award in 2004.